urban science

MDPI

Article

Climate Warming in the Eastern Mediterranean: A Comparative Analysis of Beirut and Zahlé (Lebanon, 1992–2024)

Rabih Zeinaldine * and Salem Dahech

PRODIG Laboratory, UMR 8586, Université Paris Cité, 75013 Paris, France; salem.dahech@gmail.com
* Correspondence: rabihzeineddin@hotmail.com

Abstract

The Eastern Mediterranean region is experiencing accelerated climate warming, yet localized patterns remain poorly understood, particularly in areas with complex topography. This study examines long-term air temperature trends from 1992 to 2024 at two sites in Lebanon: Beirut Airport (urban–coastal) and Houch Al Oumaraa station in Zahlé (inland–valley). Using homogeneity testing, linear regression, and the Mann–Kendall trend test, we assess trends in minimum, maximum, and mean temperatures. The results show a strong and statistically significant warming trend in Beirut, with mean temperatures rising by +0.536 °C per decade and minimum temperatures showing the steepest increase (+0.575 °C/decade). In Zahlé, the warming trend is less pronounced, particularly for maximum temperatures (+0.369 °C/decade), while minimum temperatures increased by +0.528 °C/decade. Data from fixed stations and drone-based vertical profiling in Zahlé confirmed the presence of cold-air pooling and thermal inversions, which moderate air temperatures and may contribute to a subdued warming trend. The strongest inversion recorded in 2022 reached 6.7 °C between ground level and an altitude of 500 m. In contrast, the urban heat island (UHI) effect in Beirut and Zahlé appear to drive nighttime warming, particularly in summer and early autumn months. These findings highlight the roles of topography and urbanization in shaping local climate trends.

Keywords: Zahlé; Beirut; temperature trends; UHI

check for updates

Received: 14 May 2025
Revised: 24 June 2025
Accepted: 26 June 2025
Published: 30 June 2025

Citation: Zeinaldine, R.; Dahech, S. Climate Warming in the Eastern Mediterranean: A Comparative Analysis of Beirut and Zahlé (Lebanon, 1992–2024). *Urban Sci.* **2025**, *9*, 247. https://doi.org/10.3390/urbansci9070247

Copyright: © 2025 by the authors. Licensee MDPI, Basel, Switzerland. This article is an open access article distributed under the terms and conditions of the Creative Commons Attribution (CC BY) license (https://creativecommons.org/licenses/by/4.0/).

1. Introduction

The Mediterranean Basin has been widely recognized as a global climate change hotspot, exhibiting warming trends that are significantly higher than the global average. Recent studies estimate that the region is warming 20–50% faster than the global average. This accelerated warming makes it especially vulnerable to future climate impacts [1–3]. This warming is manifested in various ways, including rising average temperatures, an increase in the frequency and intensity of heatwaves, and notable alterations in precipitation patterns [4,5]. Concrete examples underscore the severity of these trends: Malta experienced a +1.1 °C increase in mean temperature between 1951 and 2010, with accelerated warming rates recorded since the 1980s [6]. In Sfax, Tunisia, minimum temperatures rose by approximately 0.38 °C per decade during a similar period [7]. These changes are driven by global greenhouse gas emissions and intensified by regional feedback, including a reduced diurnal temperature range and warmer sea surface temperatures [8–10].

The Mediterranean's climate is also marked by substantial spatial variability due to its complex topography and maritime influences. Several studies have concluded that the highest warming rates were found in the Levantine Basin, while the central Mediterranean,

including parts of the Tyrrhenian and Ionian Seas, exhibited lower warming trends [11–13]. More studies have found that stations in the western Mediterranean have exhibited warming rates estimated between +0.2 and +0.38 °C per decade [14,15]. In contrast, Pastor et al. (2020) found that the Eastern Mediterranean Basin has experienced a warming trend of approximately 0.040 °C per year over the 38-year period analyzed (between 1982 and 2019) [16]. This rate is higher than that of the Western Mediterranean Basin, which exhibited a warming trend of about 0.035 °C per year, and the Central Mediterranean Basin, with a trend of 0.031 °C per year. In Lebanon, the study by Traboulsi et al. (2021) found that the most pronounced increases occurred during the summer season [17]. Over the study period (between 1971 and 2017), the maximum summer temperatures increased by approximately +3.83 °C, while the minimum temperatures rose by +3.53 °C. In winter and autumn, warming was more noticeable in the minimum temperatures, whereas in spring and summer, the increase in the maximum temperatures was stronger. These patterns are attributed to factors such as large-scale circulation, intensified urbanization, and diminished vegetation cover.

Furthermore, local effects, such as UHI, play a role in warming trends in the cities. Urban areas experience higher temperatures compared to their rural surroundings due to the UHI effect, which is driven by factors such as increased impervious surfaces, reduced vegetation, and anthropogenic heat release from buildings and vehicles [18]. This localized warming can significantly affect temperature trends in cities, thereby amplifying the overall warming rate in urban environments. Studies have shown that urban areas are warming at a faster pace than rural areas, a trend that is particularly evident in cities around the world. In Tunisia, studies have found that nighttime temperatures in cities like Sfax can be 4–5 °C higher than in nearby rural zones due to land use changes and infrastructure density [19]. In Paris, the temperature anomalies reach 2.5–3 °C [20]. The urban heat island effect has significantly contributed to the rise in nighttime temperatures, particularly during the summer. This localized warming due to UHI contributes to an intensification of heatwaves, increases energy demand, and can exacerbate the effects of climate change on urban populations [21]. Moreover, the UHI effect alters local climate dynamics, contributing to air quality degradation, which affects both human health and ecosystem stability [22].

This study addresses key gaps in understanding temperature trends in the Zahlé region, placing them in the broader context of Mediterranean climate change, while also comparing these trends with those of Beirut. First, it conducts a detailed trend analysis using the homogeneity, adjusted Mann–Kendall, and Sen's slope methods applied to two representative stations: Beirut Airport Station (coastal) and Houch Al Oumaraa Station (HAO) in Zahlé (inland-valley) over the 1995–2024 period in Zahlé and the 1992–2024 period in Beirut. Second, it investigates urban–rural temperature gradients through mobile temperature surveys in Zahlé, providing insight into the spatial extent and intensity of UHI effects. Finally, it investigates the factors that contribute to the cooling of the Zahlé Valley, especially the thermal inversions, through vertical measures of the air temperature and mobile measurements. The fieldwork in this study was carried out as part of our Ph.D. thesis.

2. Study Area, Data, and Methods

2.1. Study Area

The Zahlé region (Figure 1) lies in eastern Lebanon, which is located between two mountain ranges: the western and eastern chains of Lebanon. It features a complex topography, with terrain stretching across the slopes of both ranges and encompassing the Zahlé Valley, a subregion of the broader Beqaa Valley. The valley floor has gentle slopes, but the terrain becomes increasingly steep toward the east and west as elevation rises. While

the mountain summits can reach altitudes of up to 2000 m, elevations within the valley range between 870 and 920 m. The main towns in the Zahlé region include Zahlé, Chtaura, and Barr Elias. Zahlé, the capital, stands out as the most important center, hosting major financial, tourist, and cultural hubs, as well as industrial activities in its surroundings. Chtaura and Barr Elias, which are smaller in size, are primarily situated in the Beqaa Valley. Urban density is higher in the center of these towns but gradually decreases toward the outskirts. The largest population resides in Zahlé, with approximately 70,000 inhabitants. The climate is Mediterranean, and the annual mean temperature recorded for the period from 1995 to 2024 is 17.1 °C. The coldest month is January (avg. 7.2 °C), while the warmest is August (avg. 26.4 °C).

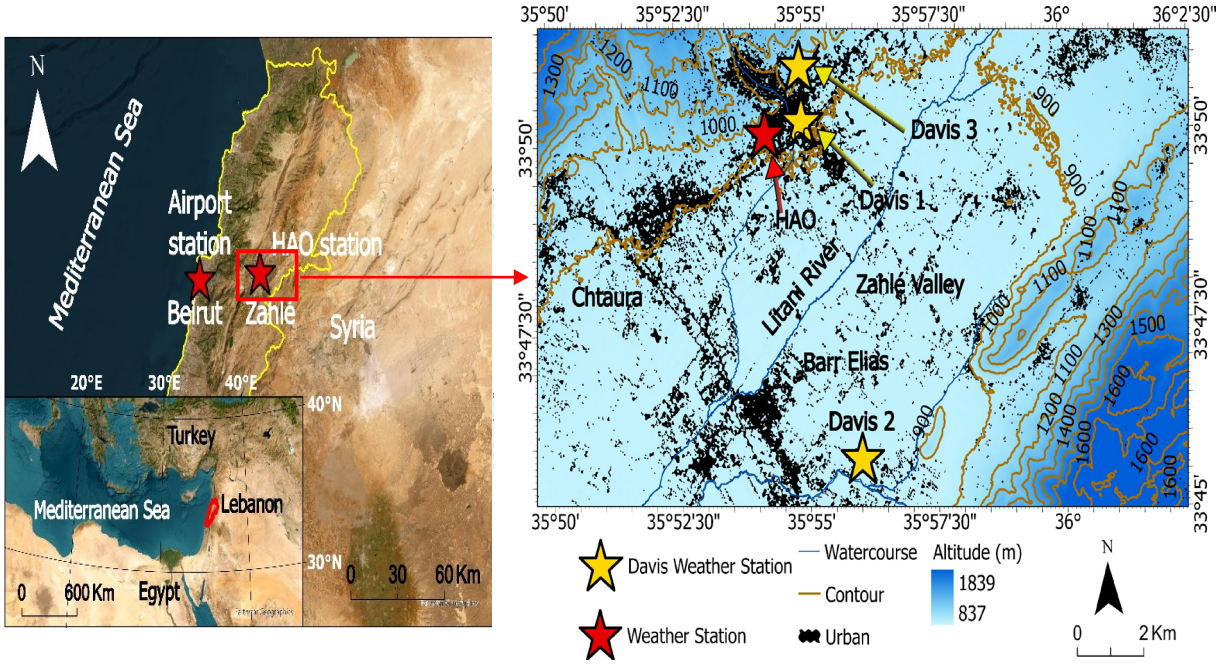


Figure 1. Location and topography of the area of study (Sources: DEM of Lebanon, Landsat 7 image, Google Earth).

2.2. Meteorological Data from Fixed Weather Stations and Gaps

This study utilized daily maximum (T max) and minimum (T min) air temperature data from the HAO station (representing Zahlé) and Beirut Airport (representing Beirut) to compute average temperatures. The data can be downloaded from the official NOAA website: www.noaa.gov (accessed on 17 April 2025). The HAO station, located at an altitude of 920 m, records temperature data at 3 h intervals. The dataset contains significant gaps during 2004, 2007, 2015, 2017, and 2018. Specifically, missing data occurred from June to October in 2004, during October in 2007, and in December 2015. More substantial gaps appeared from July to December 2017, while in 2018, only December data is available. Furthermore, incomplete records were also present for 2023 and 2024. To address these deficiencies, we used data from a Davis weather station (Davis 1), which was installed in January 2022, approximately 1 km from the HAO station in an urban location and at a comparable altitude. All temperature data for 2023 and 2024 originate from the Davis 1 station and represent actual recorded measurements. To ensure that the Davis 1 station could reliably supply missing HAO data, we compared both datasets for the year 2022. The differences in monthly mean temperatures between the two stations ranged from 0.2 °C to 0.7 °C, with an annual average temperature of 17.6 °C at the HAO station and 17.3 °C at the Davis 1 station, an overall difference of just 0.3 °C, which we considered acceptable for

data substitution (Figure 2a). Due to the data limitations, we did not calculate the annual averages for the years 2004, 2007, 2015, 2017, and 2018 at the HAO station.

The Beirut Airport station maintained consistent, uninterrupted hourly interval data recordings throughout the study period. However, for the annual temperature trend, we used data from 1992 to 2024 for this station. The HAO and Beirut Airport stations provide both sub-hourly and daily temperature data, which are available through the NOAA database. In our analysis, we used the daily data provided for these stations. For the Davis 1 station, the annual average temperature was calculated by first deriving daily T mean values using the average of daily T max and T min. The same approach was applied to the HAO and Beirut stations; since the NOAA-provided data include only daily T max and T min, we computed T mean as the average of these two values for each day. All available mean daily records from the HAO, Beirut Airport, and Davis 1 stations were utilized when generating the heatmaps.

Davis weather stations deliver reliable temperature readings at 30 min intervals and are commonly used in climate research [19,23,24]. Each temperature value is based on an unweighted average of readings taken every 2.5 s over the 30 min period (https://www.skystef.be/Davis.pdf) (accessed on 15 April 2025). These automated stations are computer-linked with initial configurations, including data transfer protocols, measurement units, selected parameters, and recording frequency. All installations followed standard meteorological practices, with temperature probes protected by white plastic shelters and mounted at a height of 2 m in unobstructed locations. The stations were newly acquired and properly calibrated prior to deployment. Verification tests were conducted via the deployment of the 3 Davis stations at the same location (the same location of Davis 1) for a 7-day period, during which intercomparison showed no significant measurement discrepancies (Figure 2b). The systems operate on solar power with battery backup, ensuring continuous data collection. Among these, the Davis 1 station remains operational at its original site, and its data were used to complete the temperature series for 2023–2024. Two additional stations (Davis 2 and Davis 3) were installed in 2022 at contrasting elevations to study thermal inversion patterns: Davis 2 at an elevation of 870 m on the valley floor and Davis 3 at an elevation of 1010 m on the western mountain slopes. This elevation differential enables a comparative analysis of temperature variations and inversion phenomena across different topographic settings in the region.

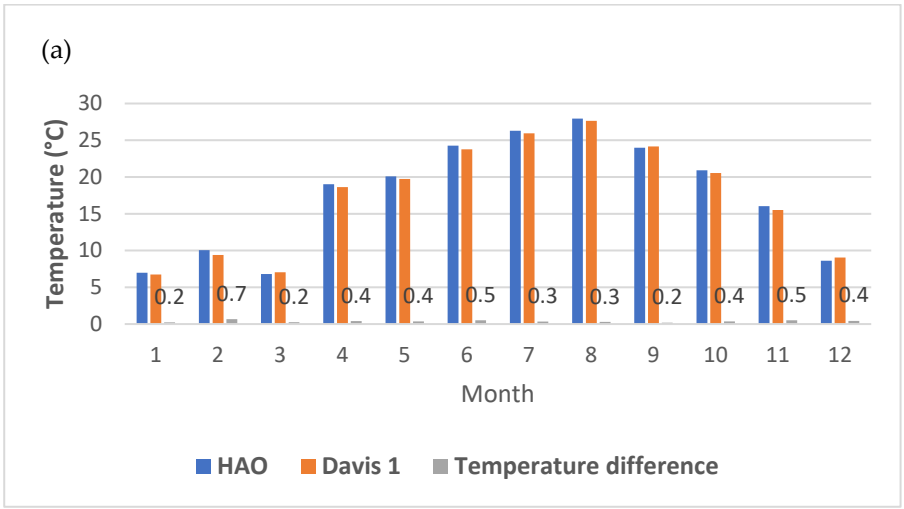


Figure 2. *Cont.*

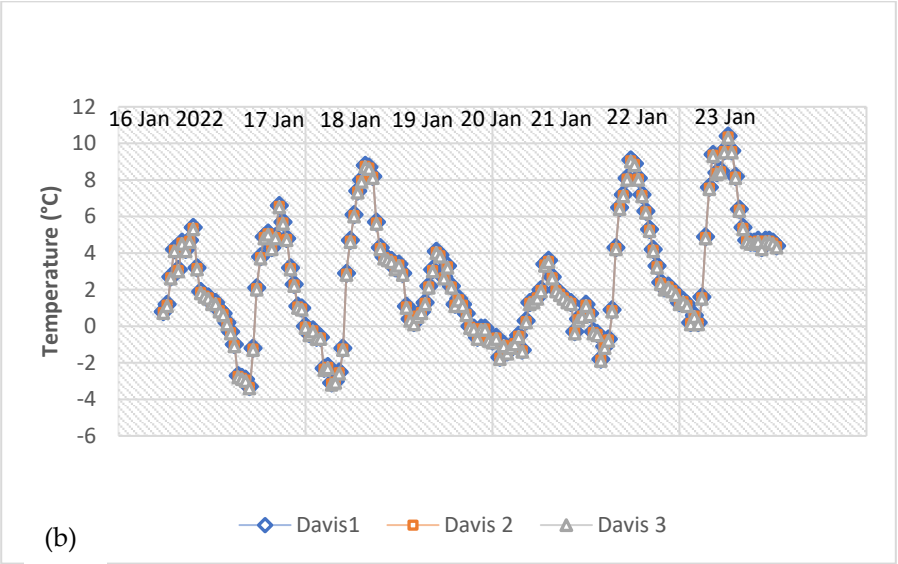


Figure 2. Comparison of monthly mean temperatures between the HAO and Davis 1 stations (**a**), and calibration test results for the three Davis weather stations used in the study (**b**). Source: Zeinaldine, R. (2024) [25].

2.3. Air Temperature Data from Mobile and Vertical Measurements

Mobile surveys were conducted at a height of 2 m above the ground at a minimum distance of 5 m from structures, with an average waiting time of one minute per point. Movement was achieved by car or motorcycle. The air temperature was measured using Tinytag sensors. These sensors have a temperature accuracy of <0.01 °C according to the technical sheet (https://assets.geminidataloggers.com/pdfs/original/3746-tgp-4017.pdf) (accessed on 10 April 2025). The calibration of these sensors was verified by comparing them with the Davis stations over a 7-day period, revealing a negligible difference of 0.01 °C, indicating that no correction was necessary. Mobile surveys took place during radiative nights between 8:30 PM and 9:30 PM. These mobile observations covered both urban and peri-urban areas and were conducted over 50 days during the summer season of 2022. To demonstrate the effect of the UHI, we conducted nighttime mobile measurements under radiative weather conditions characterized by clear skies, light winds, and dominant radiative energy exchanges, with intense solar heating during the day followed by rapid terrestrial cooling at night [26]. The measurement route crossed urban areas in the Zahlé and Bar Elias agglomerations, as well as rural zones, vegetated areas, and agricultural fields throughout the valley. To investigate thermal inversion dynamics in the valley, vertical air temperature profiles were collected using a Tinytag temperature sensor mounted on a DJI Phantom 3 Pro drone (Figure 3). The drone is manufactured by DJI (SZ DJI Technology Co., Ltd., Shenzhen, China), based in Shenzhen, China. This methodology aligns with the approach of Cordeiro et al. (2023) [27], who employed a DJI Mavic drone equipped with a similar sensor for atmospheric temperature measurements.



Figure 3. Tinytag sensor mounted on a drone used in the vertical measurement of air temperature. Source: Zeinaldine, R. (2024) [25].

The sensor was programmed to record temperature at 2 s intervals. During flights, the drone ascended to a maximum altitude of 500 m above ground level, pausing for 15 s at every 20 m interval to ensure stable measurements. Data collection occurred in the valley's lowest topographic section (870 m elevation) during the pre-sunrise period (6:00 a.m.–6:30 a.m. local time), coinciding with typical inversion conditions and prior to solar heating effects. The data were collected through the following steps:

1. The sensor was programmed to record temperature every 2 s.
2. It was then mounted on a drone.
3. A vertical flight was carried out, with pauses of 10–15 s at every 20 m of altitude. The maximum altitude reached was 500 m.
4. During the flight, we manually recorded the time and corresponding altitude (e.g., at 6:30′:42″; the altitude was 100 m) based on the altitude displayed on the drone's remote control screen.
5. For data processing, we retained one representative temperature reading for each 20 m altitude level and discarded the remaining readings.

2.4. Statistical Methods

2.4.1. Descriptive Statistical Analysis

Annual averages of maximum (T max) and minimum (T min) temperatures were computed from daily observational data. Temperature anomalies, defined as deviations from the mean, were subsequently calculated for both annual and monthly T max and T min values.

2.4.2. Homogeneity Tests

We excluded all missing data from the HAO station datasets for the annual test of homogeneity. The missing HAO station data for 2023 and 2024 were supplemented using measurements from the Davis 1 station.

The homogeneity of the annual temperature time series was evaluated using four widely recognized statistical tests designed to detect inhomogeneities: the non-parametric Pettitt's test [28], the standard normal homogeneity test (SNHT) [29], the Buishand range test [30], and the Von Neumann ratio test [31]. Discontinuity is defined here as an abrupt shift in the statistical properties (specifically, the mean) of a climate variable over time,

potentially reflecting non-climatic influences. The focus of this analysis is on discontinuities that affect annual average temperatures.

Each method has specific assumptions and strengths. The Buishand range test is a parametric method that tests for a shift in the mean under the assumption of normally distributed, independent, and identically distributed values. The Pettitt test, in contrast, is non-parametric and based on rank statistics; it is especially effective in identifying a single shift point in the middle of a time series and is sensitive to stepwise changes in the median.

The SNHT is also parametric and particularly suited for detecting a single abrupt change; it compares the mean of a segment with the mean of the entire series to evaluate the presence of a break. Finally, the Von Neumann test evaluates the randomness of a series based on the ratio of successive differences to overall variance, and deviations from randomness may indicate hidden discontinuities in the data.

The combination of these methods allows for a robust assessment of homogeneity, as each one provides complementary insights. A time series was flagged as potentially inhomogeneous if at least one test significantly rejected the null hypothesis of homogeneity. When possible, metadata such as station relocation history, changes in instrumentation, or shifts in observational protocols were consulted to support the statistical findings [32]. These metadata are critical in distinguishing between artificial and climatic causes of detected discontinuities.

2.4.3. Trend Tests

a. The trend equation

As an initial statistical method, we employed linear regression analysis to determine the temperature trends over time [33]. The general form of the regression model is $y = ax + b$, where y represents the temperature in °C, x denotes the time in years, a is the slope that indicates the rate of change, and b is the intercept that corresponds to the temperature at the start of the observed period.

This technique has been widely adopted in climatological studies [34–36] due to its clarity and ease of interpretation. The direction and magnitude of the trend can be directly inferred from the slope: a positive value ($a > 0$) indicates an increasing trend, a negative value ($a < 0$) indicates a decreasing trend, and a slope of zero ($a = 0$) suggests no significant change over time. This straightforward interpretation makes linear regression a valuable tool for identifying long-term temperature changes both visually and numerically.

b. Mann–Kendall

To assess the presence of monotonic trends in temperature variables, we applied the non-parametric Mann–Kendall trend test to the minimum, maximum, and mean temperature series. This method is widely used in climatological studies due to its robustness against non-normal data distributions and its ability to detect consistent upward or downward trends over time. Numerous studies have employed the Mann–Kendall test to investigate temperature changes across various geographic regions [37–39].

The Mann–Kendall test was used to evaluate the presence of trends in the time series by testing two competing hypotheses: the null hypothesis (H_0), which assumes the absence of any trend, and the alternative hypothesis (H_a), which suggests that a statistically significant trend exists [40]. To assess the strength of evidence against the null hypothesis, the *p*-value was calculated in percentage terms. If the computed *p*-value was less than the chosen significance level, α (commonly set at 5%), the null hypothesis was rejected in favor of the alternative, indicating a statistically significant trend. Conversely, if the *p*-value exceeded α, there was insufficient evidence to reject the null hypothesis, and no significant trend was inferred. The computations, including *p*-value estimation and hypothesis testing, were

performed using XLSTAT statistical software version 2016 (https://www.xlstat.com/en/) (accessed on 15 April 2025).

3. Results

3.1. Homogeneity

For the period of 1995–2024, the homogeneity test results for the HAO weather station reveal contrasting patterns among the three temperature parameters and identify specific years during which statistical breakpoints occurred. The T mean series shows strong evidence of non-homogeneity, with three out of four tests (Pettitt's, SNHT, and Buishand) indicating statistically significant shifts. The identified breakpoints are in 2009 (SNHT and Buishand) and 2013 (Pettitt's). Similarly, the T min series is non-homogeneous across all four tests, with breakpoints detected in 2009 (Pettitt's and Buishand) and 2022 (SNHT). In contrast, the T max series appears homogeneous, as no test identified significant change points or break years (Tables 1 and 2).

Table 1. Homogeneity tests applied to the HAO and Beirut Airport station data (significance level: 0.05).

		T mean		T max		T min	
	Test	***p*-Value**	**Homogeneity**	***p*-Value**	**Homogeneity**	***p*-Value**	**Homogeneity**
HAO Station	Pettitt's test	0.005	Non-homogeneous	0.16	Homogeneous	0.001	Non-homogeneous
	Standard normal homogeneity test (SNHT)	0.018	Non-homogeneous	0.216	Homogeneous	0.002	Non-homogeneous
	Buishand test	0.004	Non-homogeneous	0.15	Homogeneous	0	Non-homogeneous
	Von Neumann test	0.276	Homogeneous	0.23	Homogeneous	0.001	Non-homogeneous
Beirut Airport Station	Pettitt's test	<0.0001	Non-homogeneous	<0.0001	Non-homogeneous	0	Non-homogeneous
	Standard normal homogeneity test (SNHT)	<0.0001	Non-homogeneous	0.005	Non-homogeneous	<0.0001	Non-homogeneous
	Buishand test	<0.0001	Non-homogeneous	0.0008	Non-homogeneous	<0.0001	Non-homogeneous
	Von Neumann test	0	Non-homogeneous	<0.0001	Non-homogeneous	0	Non-homogeneous

The homogeneity test results for the Beirut Airport station between 1992 and 2024 indicate a clear and consistent pattern of non-homogeneity across all temperature parameters (T mean, T max, and T min). All four tests (Pettitt's, SNHT, Buishand, and Von Neumann) identify statistically significant breaks in each of the three series. The detected breakpoints for T mean are placed in 2007 across all three applicable tests, indicating a shift in the average temperature data during that year. For T max, all three tests identify a breakpoint in 2006. The T min series also shows breakpoints: 2013 (Pettitt's), 2015 (Buishand), and 2016 (SNHT) (Tables 1 and 2).

Table 2. Homogeneity tests and breakpoints.

	Test	Breakpoint		
		T mean	**T max**	**T min**
HAO Station	Pettitt's test	2013	_	2009
	Standard normal homogeneity test (SNHT)	2009	_	2022
	Buishand test	2009	_	2009
Beirut Airport Station	Pettitt's test	2007	2006	2013
	Standard normal homogeneity test (SNHT)	2007	2006	2016
	Buishand test	2007	2006	2015

3.2. Trends

Temperatures in Zahlé show a clear warming trend (Figure 4a). Over the past decade, the mean temperature has increased by 0.369 °C, the minimum temperature has increased by about 0.528 °C, and the maximum temperature has risen by around 0.284 °C. However, the low coefficients of determination for T mean and T max indicate weak linear relationships, while only T min displays a relatively stronger trend (R^2 = 0.4017). In contrast, the Beirut Airport station shows more substantial and consistent warming across all temperatures: the mean temperature has increased by 0.536 °C per decade, the maximum temperature has increased by 0.493 °C, and the minimum has increased by 0.575 °C (Figure 4b). The trends are supported by moderate to strong coefficients of determination (R^2 = 0.2695 for T max, 0.5931 for T mean, and 0.59 for T min), indicating more stable and linear warming patterns compared to the HAO station.

Annual average temperatures were calculated using both minimum and maximum values, and temperature anomalies were assessed by comparing each year's data. Before 2010, negative anomalies were more common and more intense in both locations (Figure 4c,d). Since 2010, however, positive anomalies have become more frequent and pronounced, reflecting a shift toward warmer conditions. The warmest years in Zahlé, ranked from hottest to slightly less hot, are 2010, 2021, 2020, and 2016. In Beirut, the warmest years were 2010, 2024, and 2018. As for the coldest years, Zahlé recorded its lowest temperatures in 1997, 2011, 2006, and 1995, while Beirut's coldest years were 1992, 1997, and 1993.

At the monthly scale, Beirut station shows a clearer upward mean temperature trend, as indicated by generally higher R^2 values in the linear regressions. At the HAO station (Zahlé), winter months (December, January, February) exhibit slight warming, with an average rate of 0.03 °C/year. In spring, April records the strongest warming trend at 0.1 °C/year (R^2 = 0.25), contributing to an overall seasonal warming rate of 0.06 °C/year. During summer, the average warming rate is 0.035 °C/year, with August being the warmest month (0.0449 °C/year, R^2 = 0.1107). In autumn, warming rates across September, October, and November are relatively similar, averaging 0.037 °C/year (Figure 5a,b).

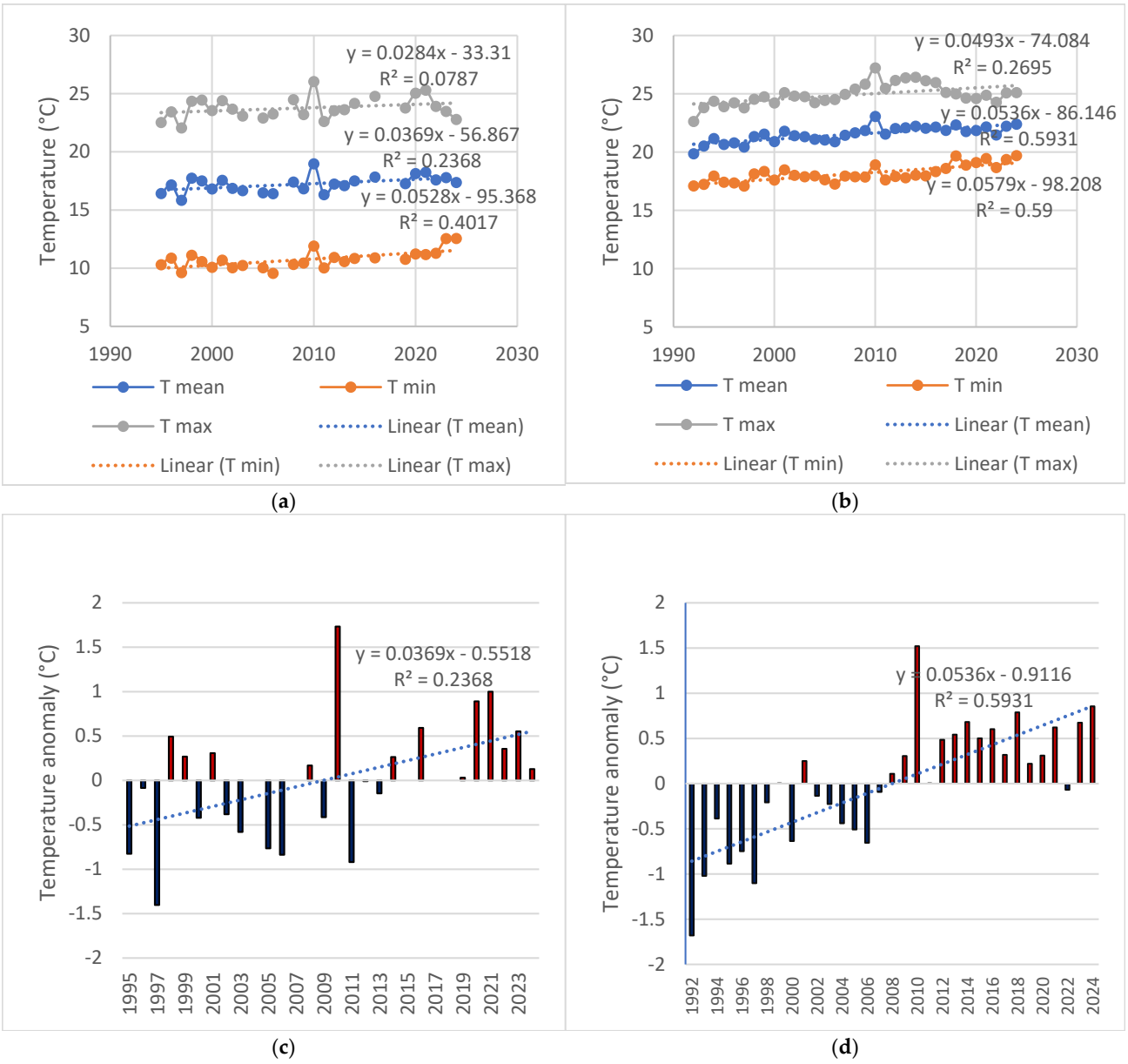


Figure 4. Annual average, maximum, and minimum temperatures values (averaged maximum and minimum temperatures) in Zahlé (**a**) and Beirut (**b**) and temperature anomaly for mean temperature in Zahlé (**c**) and Beirut (**d**) for the period of 1995–2024 for Zahlé and 1992–2024 for Beirut (missing years in Zahlé: 2004, 2007, 2015, 2017, and 2018).

At the Beirut station, winter warming is more pronounced, with an average rate of 0.053 °C/year, and February shows the strongest trend (0.07 °C/year, R^2 = 0.11). In spring, the warming rate is 0.052 °C/year, with May exhibiting the most notable increase. The summer season shows the highest warming rate, averaging 0.057 °C/year, with August standing out as the warmest month. In autumn, September and November display stronger warming trends, with a seasonal average of 0.052 °C/year (Figure 5c,d).

We applied the Mann–Kendall test to annual minimum, maximum, and mean temperature data for both stations (Table 3). At the 0.05 significance level, the results revealed a significant upward trend in T min, T max, and T mean at Beirut Airport station.

Table 3. Mann–Kendall test applied to annual mean, maximum, and minimum temperatures in Zahlé and Beirut at a significance level of 0.05. In bold: Significant values at the following level of significance: alpha = 0.05 (two-tailed test).

	Mann–Kendall	Kendall's Tau	*p* Value	Significance
HAO Station	T min	**0.43**	**0.001**	**S positive trend**
	T max	0.218	0.094	NS positive trend
	T mean	**0.366**	**0.004**	**S positive trend**
Beirut Airport Station	T min	**0.542**	**<0.0001**	**S positive trend**
	T max	**0.413**	**0.001**	**S positive trend**
	T mean	**0.617**	**<0.0001**	**S positive trend**

At the HAO station, we observed a significant upward trend in the T min and T mean, while the T max showed a statistically non-significant upward trend.

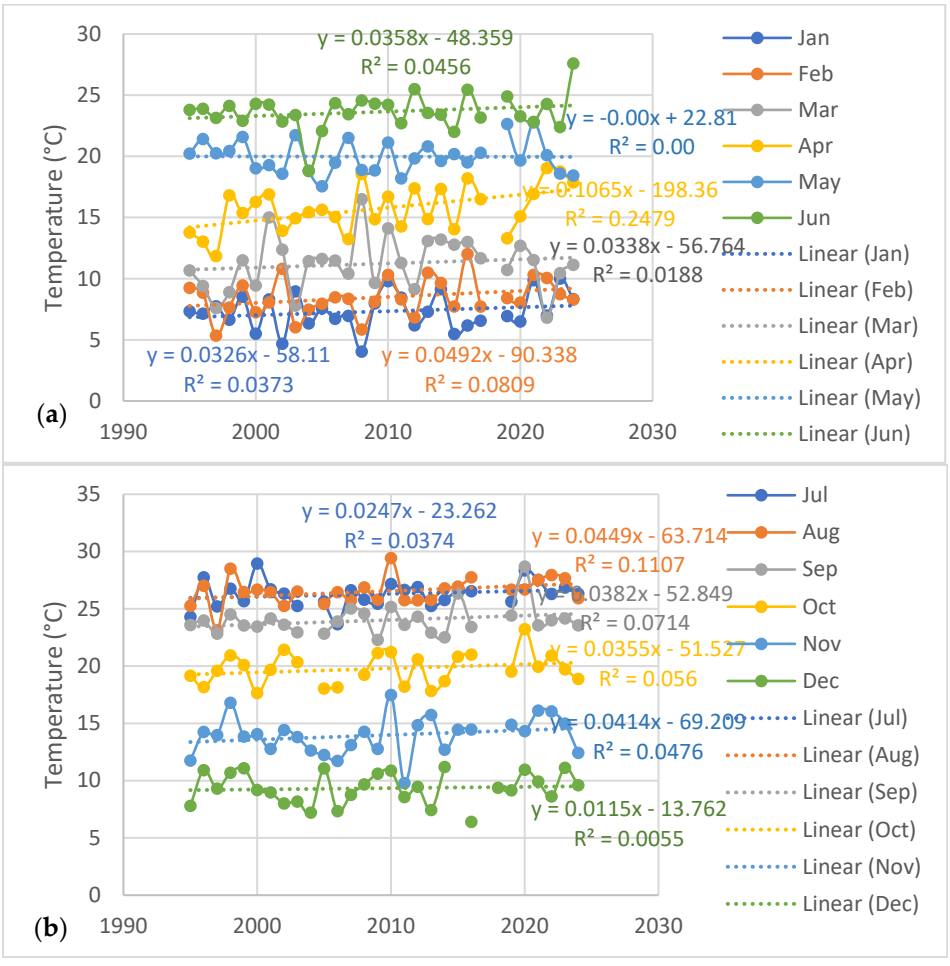


Figure 5. *Cont.*

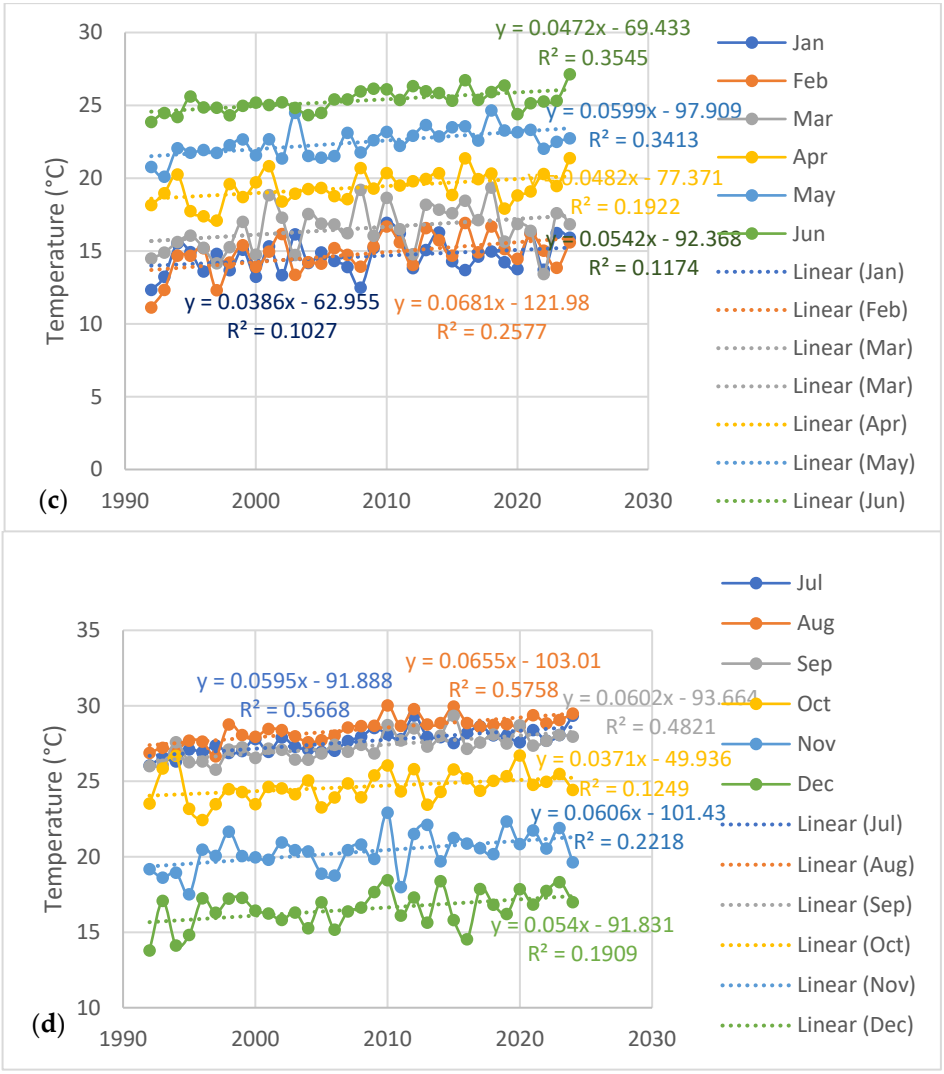


Figure 5. Monthly mean temperature values for the period of 1995–2024 in Zahlé, (**a**,**b**), as well as for the period of 1992–2024 in Beirut, (**c**,**d**) (missing years in Zahlé: 2004, 2007, 2015, 2017, and 2018).

We also ran the test on monthly T min and T max data for both stations (Table 4). At the HAO station, most months show non-significant but positive trends in both minimum and maximum temperatures, indicating a general tendency toward warming. Statistically significant warming in T min is observed in August, September, and November, suggesting that late summer and autumn are the most affected seasons. For the T max, only April shows a significant warming trend. In contrast, Beirut demonstrates much stronger and more widespread warming signals, especially in the T min, where 10 out of 12 months show statistically significant positive trends, particularly during the summer and early autumn months (July to September). The T max at Beirut also exhibits significant warming in several months, especially from May through September, although the trends are less consistent than for the T min. These findings suggest that the coastal urban environment of Beirut is experiencing more intense and statistically robust warming than the HAO station.

Table 4. Mann–Kendall test applied to monthly maximum and minimum temperatures in Zahlé and Beirut at a significance level of 0.05. In bold: Significant values at the following level of significance: alpha = 0.05 (two-tailed test), a: Trend of temperature per year in °C, S: Significant values of trend (a) at the following level of significance: alpha = 0.05 using Student's test, NS: Non-significant values of trend (a) at the following level of significance: alpha = 0.05 using Student's test.

Station	Month	T min					T max				
		Kendall's Tau	**a (°C)**	**R^2**	***p*-Value**	**Significance**	**Kendall's Tau**	**a (°C)**	**R^2**	***p*-Value**	**Significance**
HAO	January	0.124	0.046	0.07	0.344	NS positive trend	0.048	0.02	0.007	0.724	NS positive trend
	February	0.237	0.05	0.09	0.069	NS positive trend	0.136	0.05	0.05	0.304	NS positive trend
	March	0.214	0.05	0.07	0.101	NS positive trend	0.025	0.02	0.003	0.860	NS positive trend
	April	0.235	0.06	0.15	0.071	NS positive trend	**0.297**	**0.14**	**0.24**	**0.022**	**S positive trend**
	May	0.09	0.025	0.04	0.502	NS positive trend	−0.039	−0.01	0.004	0.777	NS negative trend
	June	0.163	0.06	0.11	0.214	NS positive trend	0.025	0.01	0.004	0.860	NS positive trend
	July	0.186	0.032	0.1	0.155	NS positive trend	0.032	0.015	0.006	0.817	NS positive trend
	August	**0.370**	**0.05**	**0.23**	**0.004**	**S positive trend**	0.214	0.048	0.07	0.101	NS positive trend
	September	**0.262**	**0.06**	**0.21**	**0.044**	**S positive trend**	0.039	0.026	0.017	0.777	NS positive trend
	October	0.214	0.047	0.12	0.101	NS positive trend	0.099	0.04	0.04	0.457	NS positive trend
	November	**0.325**	**0.074**	**0.21**	**0.012**	**S positive trend**	0.136	0.027	0.012	0.304	NS positive trend
	December	0.182	0.05	0.095	0.166	NS positive trend	−0.071	−0.023	0.02	0.596	NS negative trend
Beirut Airport Station	January	0.212	0.037	0.1	0.086	NS positive trend	0.167	0.04	0.08	0.179	NS positive trend
	February	**0.337**	**0.06**	**0.26**	**0.005**	**S positive trend**	**0.277**	**0.075**	**0.2**	**0.024**	**S positive trend**
	March	**0.299**	**0.05**	**0.17**	**0.014**	**S positive trend**	0.212	0.056	0.075	0.086	NS positive trend
	April	**0.241**	**0.04**	**0.18**	**0.05**	**S positive trend**	**0.246**	**0.05**	**0.12**	**0.045**	**S positive trend**
	May	**0.326**	**0.05**	**0.28**	**0.007**	**S positive trend**	**0.345**	**0.07**	**0.24**	**0.005**	**S positive trend**
	June	**0.341**	**0.046**	**0.33**	**0.005**	**S positive trend**	**0.254**	**0.048**	**0.13**	**0.039**	**S positive trend**
	July	**0.466**	**0.066**	**0.46**	**<0.0001**	**S positive trend**	**0.332**	**0.05**	**0.21**	**0.007**	**S positive trend**
	August	**0.572**	**0.077**	**0.6**	**<0.0001**	**S positive trend**	**0.394**	**0.05**	**0.2**	**0.001**	**S positive trend**
	September	**0.563**	**0.077**	**0.58**	**<0.0001**	**S positive trend**	**0.322**	**0.04**	**0.16**	**0.008**	**S positive trend**
	October	**0.333**	**0.05**	**0.16**	**0.006**	**S positive trend**	0.167	0.025	0.047	0.179	NS positive trend
	November	**0.448**	**0.078**	**0.34**	**0**	**S positive trend**	0.180	0.04	0.09	0.145	NS positive trend
	December	**0.355**	**0.067**	**0.3**	**0.004**	**S positive trend**	0.186	0.04	0.085	0.134	NS positive trend

To assess these differences throughout the year, we calculated the mean temperatures over 10-day periods across the entire dataset. The resulting heatmaps clearly illustrate the thermal disparities between the two stations.

The heatmaps for the HAO and Beirut stations illustrate distinct air temperature patterns (Figure 6). The HAO station exhibits colder winter temperatures, often dropping below 6 °C, a result of continental effects and elevation. In contrast, the Beirut station benefits from the Mediterranean Sea's moderating influence, leading to milder winters. During summer, Beirut generally records higher overall mean temperatures, while HAO experiences cooler nighttime conditions due to thermal breezes and inversions. This moderates the mean summer temperatures at HAO, even though daytime highs can reach up to 40 °C. The HAO heatmap highlights less frequent but intense heat waves, particularly in 1996, 1998, 2000, 2001, 2010, 2020, and 2023, which are visible as pronounced warm anomalies. Beirut, however, shows a clearer trend of increasing heat wave frequency and intensity, especially from 2007 onward, reflecting a stronger warming trajectory consistent with global climate trends.

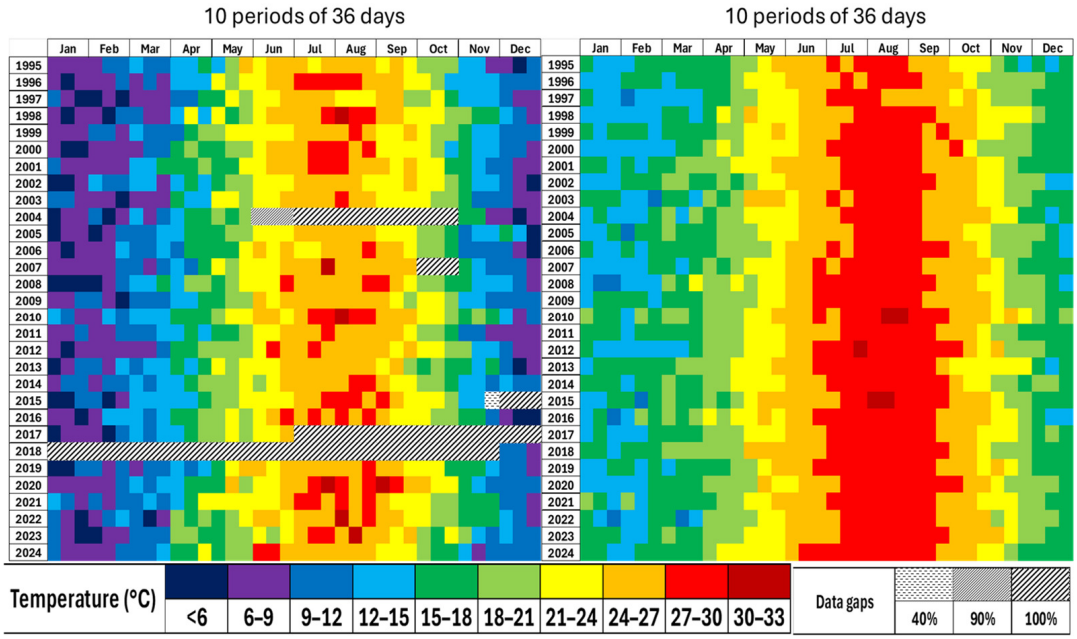


Figure 6. Heatmaps in Zahlé (**left**) and Beirut (**right**) obtained by calculating the average of the mean air temperatures of 10-day periods between 1995 and 2024.

3.3. Possible Explanations

3.3.1. Metadata

Metadata files serve as a source of supplementary information for assessing potential inconsistencies or inhomogeneities within the data series. The Beirut Airport weather station has continuously operated from its original location at Beirut–Rafic Hariri International Airport since its establishment. It is one of the longest-standing official meteorological stations in Lebanon, and all available records confirm that the station has never been relocated or significantly altered in its position over the years.

Similarly, the Houch Al Oumaraa weather station, located in the Beqaa Valley, has been consistently operational since 1994. There is no evidence or documentation suggesting any relocation since its inception, indicating that the station has remained fixed at its original site throughout its operational history.

3.3.2. Large-Scale Circulation

Between 1995 and 2025, the Eastern Mediterranean has experienced noticeable warming, and much of this change can be traced back to the influence of large-scale atmospheric circulation patterns. These patterns, including the North Atlantic Oscillation (NAO) and the Mediterranean Oscillation Index (MOI), have shaped not just how warm or cold the region gets but also how frequently it experiences extreme heat or dry spells.

A positive phase of the NAO corresponds to a stronger than average pressure gradient, leading to intensified westerlies and storm tracks that have shifted northward. This typically results in mild and wet winters in northern Europe and cooler, drier conditions in southern Europe and the Mediterranean. Conversely, a negative phase weakens the pressure gradient, reducing the westerly flow and leading to colder winters in northern Europe and wetter conditions in the Mediterranean [41–43].

The MOI, which measures the pressure difference between western and eastern parts of the region, also plays a role. Several studies have highlighted the important role of the Mediterranean MOI in shaping climate variability across the Mediterranean region. The MOI is closely linked to fluctuations in precipitation and temperature, with low MOI phases generally associated with wetter and cooler conditions, particularly in the southern and

eastern parts of the basin. Compared to the NAO, the MOI provides more localized insights, especially in regions where the NAO's influence weakens. Research also shows that the impact of the MOI varies seasonally and can interact with other large-scale patterns like ENSO, thereby enhancing its effect on regional droughts and temperature extremes [44–47].

We used a Pearson correlation matrix to assess the relationship between annual mean temperatures and the MOI. The results show a modest positive correlation in Beirut ($r = 0.212$) and a weaker one in Zahlé ($r = 0.103$). However, we did not find any statistically significant link between air temperature and the NAO at either station, with correlation values of $r = -0.06$ for Beirut and $r = 0.02$ for Zahlé.

3.3.3. Local Factors

a. UHI effect in Beirut

The UHI effect refers to the phenomenon in which urban areas experience higher air temperatures than their surrounding rural regions, primarily due to human activities and land surface modifications. This temperature difference is driven by factors such as the extensive use of heat-absorbing materials like asphalt and concrete, reduced vegetation cover, and waste heat from buildings, vehicles, and industrial processes. As a result, cities often retain more heat during the day and release it more slowly at night, leading to consistently warmer conditions. The UHI effect can significantly influence local climate measurements by elevating air temperatures, particularly at night [48]. Several studies have focused on the UHI effect in Beirut. For example, Faour et al. (2023) analyzed nighttime satellite imagery to assess changes in the land surface temperature (LST) between 1990 and 2020. Their findings showed a noticeable warming trend, with urban areas experiencing an average increase of about 1.26 °C and vegetated zones warming by approximately 1.10 °C [49]. Similarly, Kaloustian and Diab (2015) reported significantly higher air temperatures in urban Beirut, noting differences of up to 6 °C during summer months compared to nearby vegetated areas [50]. The UHI effect in Beirut may partially explain the stronger warming trend observed in minimum temperatures, especially when compared to the Zahlé region, which is less urbanized and thus less affected by this phenomenon.

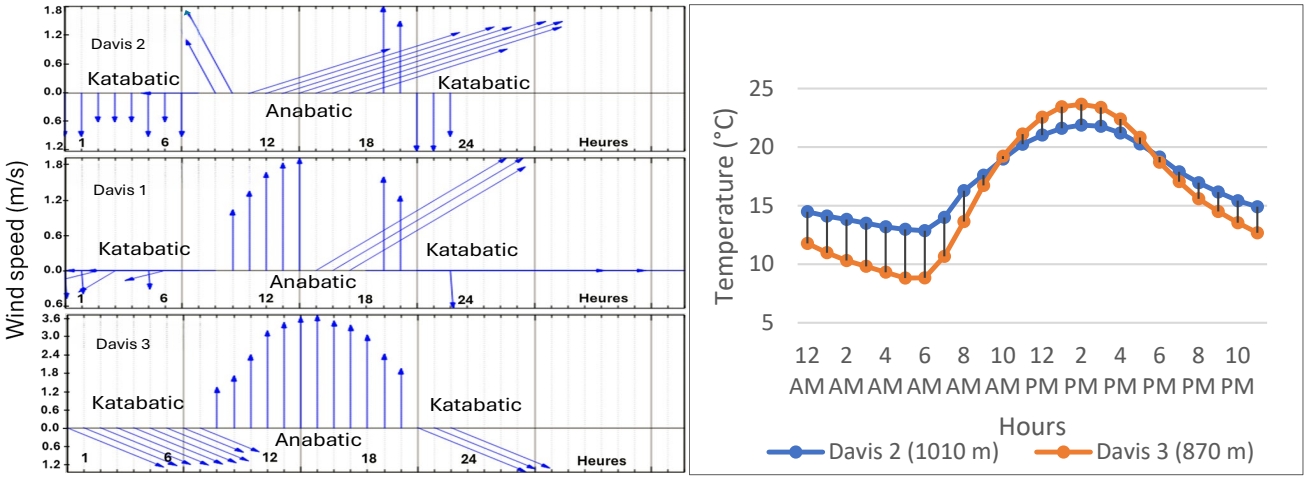
b. Local climate of Zahlé

The Zahlé region, with its contrasting topography, exhibits a local climate marked by a thermal breeze circulation regime. Two primary types of thermal breezes dominate this area: anabatic and katabatic flows. These phenomena, which were thoroughly described by Zeinaldine and Dahech, (2023) [51], are commonly observed under radiative weather conditions and clear skies typical of summer, spring, and autumn, but they can also occur during the winter season. These breezes play a crucial role in ventilating the Zahlé Valley, particularly through katabatic flows at night, which transport cool and moist air down to the valley floor. This process fosters the formation of cold air pools and leads to thermal inversions. The Davis weather stations installed in the region have recorded these thermal breeze events. Specifically, the cooling effect has been assessed by comparing temperature data between Davis 2, located at the valley floor (870 m), and Davis 3, situated on a slope at 1010 m. In addition, vertical measurements taken in 2022 within the valley floor further confirmed the presence of thermal inversions.

Cooling Factors: Thermal Breezes and Inversions

Thermal breezes are predominant in Zahlé. An analysis of 2022 wind data from the Davis stations shows that the nocturnal katabatic breeze generally blows from the north and is strongest at the higher-altitude Davis 3 station, blowing at an average speed of 1.2 m/s. In contrast, this breeze is much weaker at the other stations, averaging only 0.6 m/s at the Davis 1 and 2 stations.

Conversely, the daytime anabatic breeze reaches its peak speed at the Davis 3 station, flowing from the south (S) and peaking at 3.6 m/s around 3 PM (Figure 7a). These thermal breezes were observed throughout 2022, occurring more frequently during the summer season.



(**a**) (**b**)

Figure 7. Anabatic and katabatic breezes observed in Zahlé in 2022 through 3 Davis weather stations (**a**); Evolution of hourly air temperature at the Davis 2 and Davis 3 stations in Zahlé in 2022 (**b**). The arrows in Figure (a) indicate the wind direction 'blowing to'. Location of weather stations in Figure 1. Source: Zeinaldine, R. (2024) [25].

Thermal inversions in valleys are primarily caused by a radiative deficit at the surface during the night. They typically occur under calm weather conditions and clear skies and often dissipate in the morning [52,53]. Local topography amplifies this inversion phenomenon: cold air moves downslope by advection and accumulates in depressions [54]. Thermal inversions are frequently observed in the Zahlé Valley. They occur during radiative nights under clear skies and are intensified by the topographic effect, which promotes cold air accumulation at the valley floor.

Weather stations located at different altitudes (Davis 3 and Davis 2) provide information on temperature inversions. The average temperature is lower at the Davis 3 station throughout the night, until 9:30 a.m. At that point, due to solar warming, the temperature in the valley surpasses that on the slope. The thermal inversion resumes its influence after 6:00 p.m., and the valley becomes colder than the slope again. In 2022, the maximum average temperature difference measured between these two stations occured at 5:00 a.m., reaching 4.4 °C (Figure 7b).

In addition, 40 vertical air temperature profiles were taken on the valley floor between April and August 2022 (6:00–6:30 a.m. local time). Thermal inversions were present on all 40 days, with varying intensities. The strongest inversion was recorded on 4 June, with a 6.7 °C difference between ground level and 500 m altitude (Figure 8).

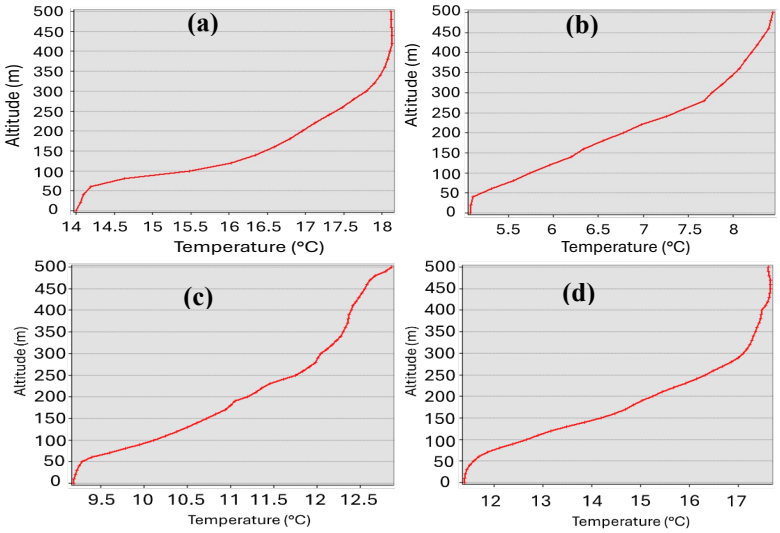


Figure 8. Vertical air temperature profiles measured in Zahlé's valley floor on 23 April (**a**), 8 May (**b**), 13 May (**c**), and 4 June (**d**) 2022. Source: Zeinaldine, R. (2024) [25].

The higher frequency of these factors in summer does not explain the more pronounced warming trend observed in Zahlé during this season compared to winter. This is likely due to the influence of additional factors. In fact, these local topoclimatic phenomena typically occur under stable atmospheric conditions that frequently occur in summer and are often associated with anticyclonic systems at higher altitudes, which create favorable conditions for their development. In contrast, winter in Zahlé is generally influenced by low-pressure systems characterized by colder temperatures (especially in December and January), stronger synoptic winds, and frequent rainfall or snowfall [17]. These conditions inhibit the formation of topoclimatic phenomena in the winter season and may explain the relatively weak warming trend compared to the summer season (Figure 5). However, these cooling factors in the Zahlé Valley, added to UHI in Beirut, may help to partially explain the difference in air temperature trends between Zahlé and Beirut, particularly the more pronounced increase observed in Beirut. Regarding the non-significant trend in T max for Zahlé, we clarify that the final dataset used for the trend analysis comprises 26 complete years between 1995 and 2024, excluding years with substantial data gaps (2004, 2007, 2015, 2017, and 2018). This sample size meets the minimum requirements for applying the Mann–Kendall test in climatological studies. This trend may be attributed to the influence of local topographic and atmospheric processes, such as thermal inversions and valley breezes, which increase interannual variability and potentially mask the expression of long-term warming in T max.

Warming Factor: UHI

Despite the presence of thermal breezes and valley ventilation, urban heat islands (UHIs) are still detected in the built-up areas of the region. The UHIs in Zahlé (altitude 930 m) and Barr Elias (altitude 880 m) were investigated through nighttime mobile air temperature measurements (conducted between 8:30 p.m. and 9:45 p.m. local time) (Figure 9). The survey route crosses diverse land uses, such as industrial zones, residential neighborhoods, arable lands, and vegetation areas of the valley. The results reveal temperature variations across different areas of the Zahlé and Barr Elias agglomerations, relative to the reference points where the highest temperatures were observed. The map clearly indicates that all urban or built-up areas exhibit relatively higher temperatures. In Zahlé, measurements showed an urban–rural temperature difference of 2.7–4.4 °C, while in Barr Elias, the contrast reached up to 4.5 °C. The urban areas have fewer green areas compared with the

valley, which is dominated by agriculture. As a result, the heat absorbed by large, hard surfaces during the day is released back into the environment at night. These mobile measurement findings are supported by data from the Davis 1 station, located in an urban area in Zahlé, and the Davis 2 station, located in a rural area in the valley, during the summer of 2022 (June, July, and August). These stations recorded a mean temperature difference of approximately 3 °C at 9 p.m., which is consistent with the results obtained from our mobile observations (Figure 10).

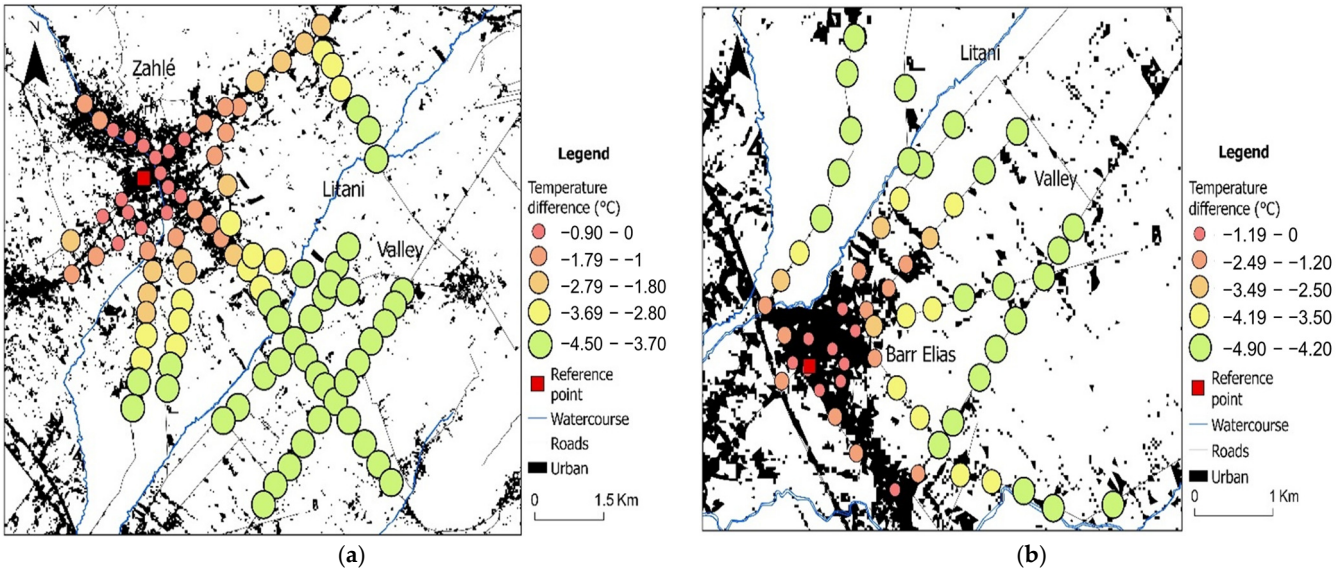


Figure 9. Spatial distribution of average nighttime air temperatures at 2 m above ground level (in °C) in the Zahlé agglomeration and the rural regions of Zahlé Valley, based on five series of mobile measurement campaigns conducted under radiative conditions on 20 July 2022, 22 July 2022, 25 July 2022, 30 July 2023, and 2 August 2023 between 8:30 p.m. and 9:45 p.m. (**a**); and in the Barr Elias agglomeration in the Zahlé Valley based on five series of mobile measurement campaigns conducted under radiative conditions on 27 June 2022, 28 June 2022, 1 July 2022, 10 July 2023, and 10 August 2023 between 8:30 p.m. and 10:00 pm. (**b**); 1 min average per point, measurements taken by car; background: built-up surfaces of the Zahlé and Barr Elias agglomerations derived from the processing of a 2017 LANDSAT 8 image.

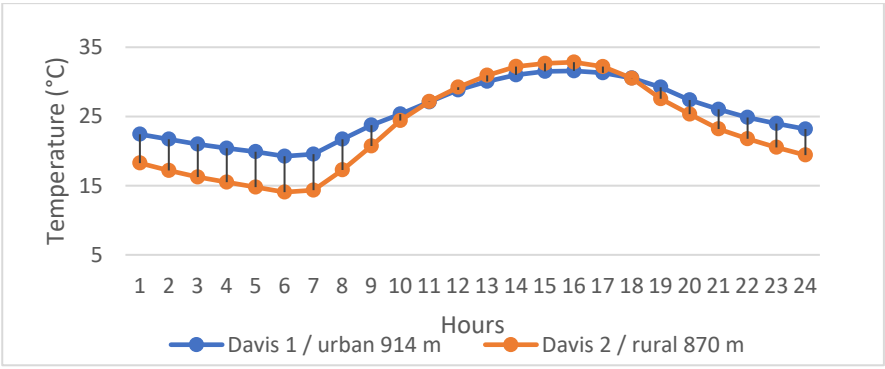


Figure 10. Evolution of hourly air temperature at the Davis 1 (urban) and Davis 2 (rural) stations in Zahlé during the summer season of 2022. Source: Zeinaldine, R. (2024) [25].

These temperature differences are notably high for relatively small urban agglomerations compared to larger cities like Beirut. This can be attributed to the nocturnal katabatic breeze in the Zahlé region, which drives cold air accumulation at the valley floor, creating a cold air pool. As a result, rural areas cool more efficiently, amplifying the thermal

contrast with urban zones. A similar study by Bokwa et al. (2015) conducted in Krakow (Poland) concluded that in cities with complex topography, local relief is a major driver of temperature patterns and should be considered alongside urbanization when assessing UHI [55].

The comparison of the urban fabric and land surface temperature (LST) in Zahlé City between 2002 and 2023 reveals a clear and significant intensification of the UHI effect driven by urban expansion. In 2002, urban areas were relatively compact and concentrated, with LST values predominantly ranging between 20.1 °C and 24.5 °C and localized hotspots barely exceeding 25 °C. By 2023, urban sprawl had expanded in all directions, resulting in a denser and more fragmented urban pattern. This spatial growth is closely mirrored by a rise in surface temperatures, with maximum LST values reaching up to 27.9 °C. The hottest zones in 2023 are largely co-located with the newly urbanized areas, where previously cooler surfaces such as vegetation or bare soil have been replaced by impervious materials that absorb and retain heat (Figure 11).

Urban growth in Beirut and Zahlé has followed very different paths in recent decades, shaped by their size and location and the impact of refugee movements. In Beirut, the Greater Beirut urban area grew steadily, reaching approximately 2.2 million inhabitants by 2015 and peaking around 2.4 million in 2023 (Population estimates for Beirut, Lebanon, 1950–2015). Faour and Mhawej (2014) [56] reported that between 1963 and 2010, the city's urban area expanded at an average rate of 1.8 km^2 per year, mainly along the coastline and eastern foothills, leading to significant green space loss—especially from 2003 to 2010—and generating high-density, vertical growth accompanied by informal settlement expansion. In contrast, the Zahlé region saw 68% growth in its population from 142,000 in 2000 to 238,000 in 2015, a rise that was largely driven by Syrian refugees after the war in 2011. Urban expansion in Zahlé between 2002 and 2023 has followed a more dispersed pattern: the northwest saw residential development with banks and restaurants, while the southeast industrial zone experienced ongoing investment in industrial and commercial infrastructure, plus new refugee camps (Figure 10). Unlike Beirut's densely packed urban environment, Zahlé retains a more horizontal urban form and lower population density, although growing pressure in both residential and industrial zones signals increasing urbanization. This increased urbanization can contribute to the warming in the two regions by intensifying the UHI effect.

Additionally, the late cessation of the sea breeze in Beirut (after 10 p.m. in summer) plays a role in nighttime warming within the city [25]. The sea breeze persists late into the evening or night, and it transports relatively warmer and more humid maritime air over the urban area. This influx of warmer air inhibits the normal radiative cooling of the city's surface and atmosphere, leading to higher nighttime temperatures. Consequently, the delayed cessation of the sea breeze contributes to the urban heat island effect in Beirut by maintaining elevated temperatures overnight. In contrast, the anabatic breeze in Zahlé fades early, around 8 p.m. (in summer), and is soon replaced by the katabatic breeze at approximately 8:30 p.m., following a brief period of nocturnal reversal. This transition initiates a cooling process as cold air descends from the mountain tops into the valley, forming a thermal inversion pool that lasts until about 11 a.m., thereby contributing to the valley's cooling. After 11 a.m., solar radiation breaks down the inversion layer, ending this cooling effect. These events occur throughout the year but are more frequent in summer due to the calm atmospheric conditions that favor the development of these local topoclimatic phenomena [25].

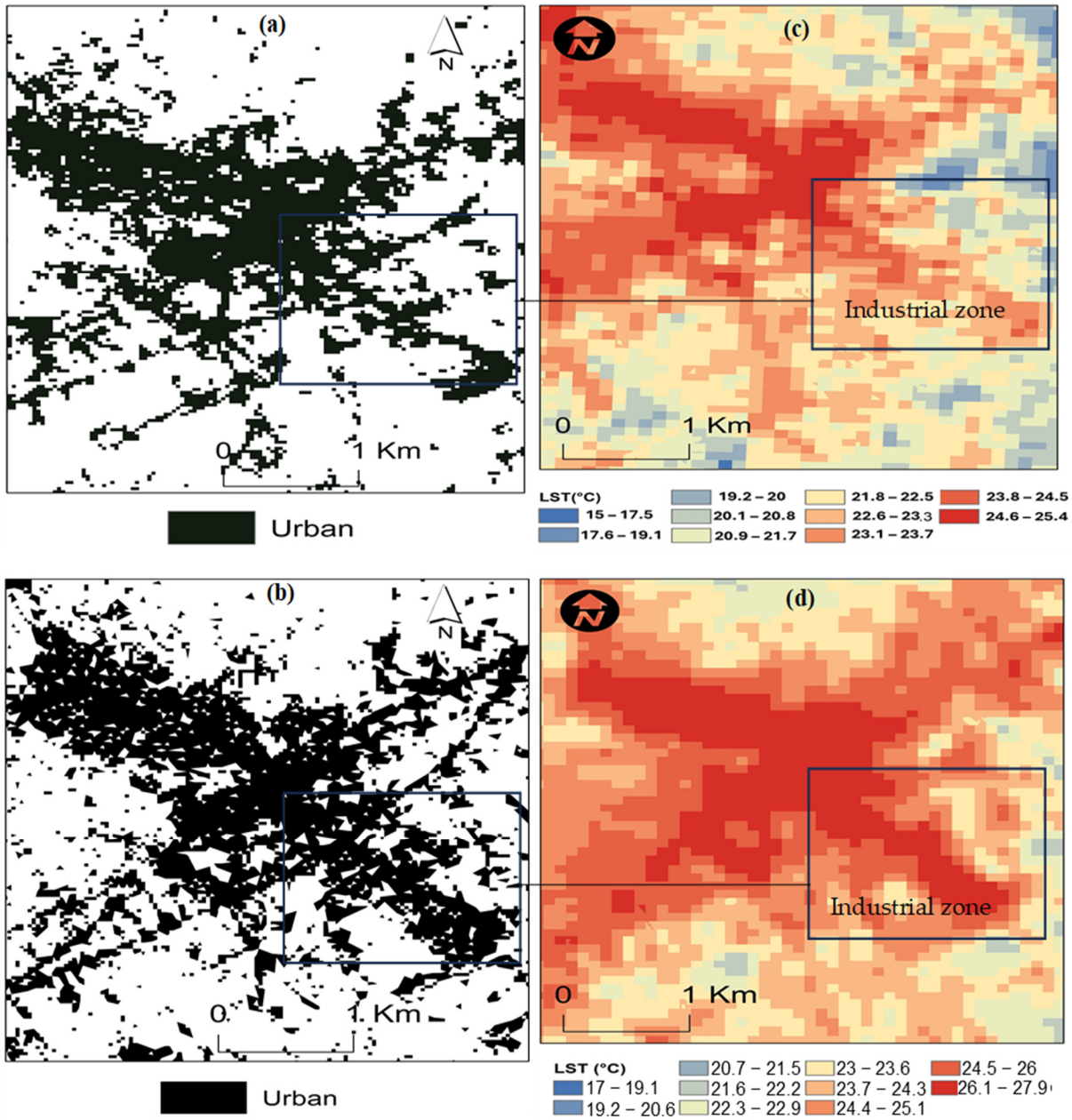


Figure 11. Changes in built-up areas in Zahlé City between 2002 (**a**) and 2023 (**b**), as well as the evolution of the urban heat island effect between 2002 (**c**) and 2023 (**d**). Sources: supervised classification of two Landsat images (Landsat 7 and Landsat 8, 30 m resolution) and treatment of thermal bands B10, B11, B12, B13, and B14 from nighttime Aster TIR satellite images taken in July 2002 and July 2023. Source: Zeinaldine, R. (2024) [25].

4. Discussion

The analysis of temperature data from the HAO station was constrained by periods of missing data, which limited our ability to conduct a complete annual analysis for the Zahlé region. Despite this limitation, the study focused on a 30-year span (1995–2024) in HAO and a 33-year span in Beirut (1992–2024), providing insights into the warming trends in Lebanon and highlighting regional climatic differences.

The temperature trends observed in Beirut and Zahlé align with broader patterns documented across the Mediterranean, highlighting the significant roles of urbanization and topography. A comprehensive analysis revealed that urban centers in the Mediterranean and Middle East–North Africa region exhibit higher warming rates, averaging

0.43 °C per decade, compared to rural areas, which average 0.36 °C per decade [15]. This disparity underscores the influence of urban heat island effects, particularly in densely populated coastal cities like Beirut. In contrast, inland areas with complex terrains, such as Zahlé, demonstrate moderate warming trends, a phenomenon that is also observed in other Mediterranean locales. For instance, Costanzini et al. (2024) [57] compared temperature records from the urban Modena Geophysical Observatory and the rural Mount Cimone Observatory in Italy and found that urbanization contributed significantly to increased temperatures in Modena, while the rural site exhibited more stable trends. Compared to the small Mediterranean city of Dubrovnik in Croatia, where Boras et al. (2024) [58] reported a marked intensification of urban heat load in both extreme and future climate scenarios, the urban heat island effect in Zahlé remains relatively moderate in intensity, with nighttime urban–rural temperature differences reaching 2.7 to 4.5 °C. However, similar to those of Dubrovnik, our results show that urban expansion in Zahlé has led to a noticeable increase in localized warming, particularly during summer nights. More studies, such as those conducted in Xanthi (Greece), Bari (Italy), Kozani (Greece), and Gabes (Tunisia), have reported UHI intensities comparable to those observed in Zahlé, confirming that small- to medium-sized Mediterranean cities can exhibit significant urban–rural temperature differences, often ranging between 2 and 5 °C [59–62].

Furthermore, high-resolution regional climate simulations projected that cities like Rome and Thessaloniki could experience an increase of approximately 1.5–3 °C in average minimum temperatures by 2100 due to urbanization, with a notable rise in the number of tropical nights [63]. These findings are consistent with the observed diurnal asymmetry in Beirut, where nighttime temperatures are rising more rapidly, likely due to urban heat retention. On a broader scale, Pastor et al. (2020) [16] reported sea surface temperature increases of +0.040 °C/year in the Eastern Mediterranean, comparable to the +0.493 °C/decade T mean increase observed in Beirut. The heat moderation observed in Zahlé aligns with results in Kraków, Poland [55], as well as those in the Italian and UK highlands [38], both of which emphasize the role of valley morphology in buffering warming. Additionally, our findings are consistent with those of Traboulsi et al. (2021) and Dahech and Beltrando (2012) [7,17], who documented significant warming trends in Mediterranean urban settings. Similar to other study results in Beirut, our study found a marked rise in both maximum and minimum temperatures, particularly during summer months, reflecting the influence of atmospheric circulation and urban heat dynamics. Likewise, the pronounced increase in minimum temperatures observed in Beirut corresponds with the trends reported in Sfax, where urbanization played a key role in nighttime warming.

These findings have important implications for regional climate adaptation planning. In coastal urban areas like Beirut, where warming trends are amplified by urban heat island effects, local authorities should prioritize UHI mitigation strategies, such as increasing green infrastructure, implementing reflective building materials, and enforcing zoning regulations that reduce surface sealing. In inland regions like Zahlé, which are characterized by topographic cooling due to thermal inversions, site-specific monitoring systems should be enhanced to better detect microclimatic variability, which is often missed by broader climate models. Incorporating these microclimatic dynamics into regional risk assessments can lead to more effective heat health warnings, energy planning, and agricultural adaptation. Furthermore, the deployment of dense sensor networks in diverse terrain can improve the resolution and relevance of climate data for regional policymaking.

Future research should aim to address the limitations posed by data gaps, particularly those at the HAO station, by deploying one or more high-quality Automated Weather Stations. This could help fill temporal gaps and provide redundancy in case of main station failures. Additionally, extending the analysis to include other locations across Lebanon

would help generalize the observed contrast. Further investigations could also focus on the role of topographic and microclimatic factors, such as thermal inversions, urban heat island effects, and local wind systems, in modulating air temperature. Deploying mobile measurement campaigns and high-resolution climate modeling could provide deeper comprehension into intra-regional variability and help quantify the specific contribution of valley dynamics to observed temperature trends. Such approaches would improve climate risk assessments at the local scale and inform targeted adaptation strategies in vulnerable areas like Beirut and the Zahlé region.

5. Conclusions

This work examined air temperature trends at two contrasting sites in Lebanon: the Beirut Airport (coastal, urban) and Houch Al Oumaraa (HAO) in Zahlé (inland valley) over the periods of 1992–2024 and 1995–2024, respectively. Using homogeneity testing, linear regression, and the Mann–Kendall method, the analysis revealed a statistically significant warming trend at both stations, but with notable spatial variability in magnitude and structure.

In Beirut, the mean temperature increased by 0.536 °C per decade, with maximum and minimum temperatures rising by 0.493 °C and 0.575 °C per decade, respectively. The warming was consistent across months and statistically significant in nearly all cases, particularly for the T min, where 10 out of 12 months showed significant trends. These findings reflect possible strong urban heat island (UHI) effects, which are amplified by dense urban infrastructure and proximity to the sea.

In contrast, Zahlé (HAO station) exhibited lower and more variable warming rates. The mean temperature rose by 0.369 °C per decade, the T max rose by 0.284 °C, and the T min rose by 0.528 °C. While the Mann–Kendall test confirmed a significant upward trend for the T min and T mean, T max trends were not statistically significant. A seasonal analysis showed that spring (especially April) and late summer to autumn (August–November) are the periods most affected by warming in Zahlé.

Mobile nighttime measurements and drone-based vertical profiles conducted in Zahlé revealed temperature inversions and katabatic flows, with cold air pooling leading to nighttime cooling. They also studied the UHI effect in the Zahlé region's main agglomerations.

Homogeneity tests also showed distinct breakpoints in the temperature series. For Beirut, a major shift occurred around 2006–2007 across all parameters. In Zahlé, the T min showed breakpoints in 2009 and 2022, suggesting localized shifts, possibly related to land use or observational changes.

In summary, this study confirms that urbanization, topography, and microclimatic processes play a role in modulating regional climate change impacts. In Beirut, the UHI effect is more intense and persistent, with nighttime temperature differences reaching up to 6 °C between urban and surrounding vegetated zones. This is largely driven by dense urbanization, impervious surfaces, anthropogenic heat emissions, and the late cessation of the sea breeze, which limits nocturnal cooling. In contrast, Zahlé exhibits a weaker UHI effect, with urban–rural temperature contrasts ranging from 2.7 to 4.5 °C. Despite ongoing urban expansion, Zahlé's lower urban density and valley setting promote nocturnal katabatic flows and cold air pooling, which facilitate more efficient nighttime cooling in rural areas. Although these topoclimatic mechanisms enhance the thermal contrast between rural and urban areas, they also help to moderate the overall urban heat island (UHI) effect. This contributes to the lower and more variable warming trends observed in Zahlé, in contrast to the stronger and statistically more consistent trends recorded in Beirut.

These results underscore the importance of localized climate monitoring and policy responses tailored to specific topographic and urban conditions. For effective climate

adaptation in the Mediterranean, strategies should combine macro-scale climate projections with fine-scale observations, particularly in urban and valley settings. Strengthening local meteorological infrastructure and integrating microclimate data into urban planning tools will be essential to enhance resilience against future warming.

Author Contributions: Conceptualization, S.D.; methodology, R.Z. and S.D.; software, R.Z.; validation, S.D.; formal analysis, R.Z.; investigation, R.Z. and S.D.; resources, R.Z. and S.D.; data curation, R.Z.; writing—original draft preparation, R.Z.; writing—review and editing, R.Z. and S.D.; supervision, S.D. All authors have read and agreed to the published version of the manuscript.

Funding: This research received no external funding.

Data Availability Statement: Data are contained within the article.

Acknowledgments: The authors thank the PRODIG UMR 8586 laboratory for providing the Davis weather stations and the equipment needed for car survey measurements. All individuals included have consented to the acknowledgement.

Conflicts of Interest: The authors declare no conflicts of interest.

References

1. Giorgi, F. Climate change hot-spots. *Geophys. Res. Lett.* **2006**, *33*, 101029. [CrossRef]
2. Tuel, A.; Eltahir, E.A.B. Why Is the Mediterranean a Climate Change Hot Spot? *J. Clim.* **2020**, *33*, 5829–5843. [CrossRef]
3. Di Bernardino, A.; Casadio, S.; Iannarelli, A.M.; Siani, A.M. Temperature Trends and Influence of the Base Period Selection on Climate Indices in the Mediterranean Region Over the Period 1961–2020. *Int. J. Climatol.* **2024**, *44*, 5969–5985. [CrossRef]
4. Lionello, P.; Scarascia, L. The relation between climate change in the Mediterranean region and global warming. *Reg. Environ. Change* **2018**, *18*, 1481–1493. [CrossRef]
5. Zittis, G.; Bruggeman, A.; Lelieveld, J. Revisiting future extreme precipitation trends in the Mediterranean. *Weather. Clim. Extrem.* **2021**, *34*, 100380. [CrossRef]
6. Galdies, C. Temperature trends in Malta (central Mediterranean) from 1951 to 2010. *Meteorol. Atmos. Phys.* **2012**, *117*, 135–143. [CrossRef]
7. Dahech, S.; Beltrando, G. Observed temperature evolution in the City of Sfax (Middle Eastern Tunisia) for the period 1950–2007. *Clim. Change* **2012**, *114*, 689–706. [CrossRef]
8. Dai, A.; Trenberth, K.E.; Karl, T.R. Effects of Clouds, Soil Moisture, Precipitation, and Water Vapor on Diurnal Temperature Range. *J. Clim.* **1999**, *12*, 2451–2473. [CrossRef]
9. Deser, C.; Alexander, M.A.; Xie, S.-P.; Phillips, A.S. Sea Surface Temperature Variability: Patterns and Mechanisms. *Annu. Rev. Mar. Sci.* **2010**, *2*, 115–143. [CrossRef]
10. Intergovernmental Panel on Climate Change (IPCC). *Climate Change 2013—The Physical Science Basis: Working Group I Contribution to the Fifth Assessment Report of the Intergovernmental Panel on Climate Change*; Cambridge University Press: Cambridge, UK, 2014. [CrossRef]
11. Pastor, F.; Valiente, J.A.; Palau, J.L. Sea Surface Temperature in the Mediterranean: Trends and Spatial Patterns (1982–2016). In *Meteorology and Climatology of the Mediterranean and Black Seas*; Vilibić, I., Horvath, K., Palau, J.L., Eds.; Springer International Publishing: Cham, Switzerland, 2019; pp. 297–309. [CrossRef]
12. Juza, M.; Tintoré, J. Multivariate Sub-Regional Ocean Indicators in the Mediterranean Sea: From Event Detection to Climate Change Estimations. *Front. Mar. Sci.* **2021**, *8*, 610589. [CrossRef]
13. García-Monteiro, S.; Sobrino, J.A.; Julien, Y.; Sòria, G.; Skokovic, D. Surface Temperature trends in the Mediterranean Sea from MODIS data during years 2003–2019. *Reg. Stud. Mar. Sci.* **2022**, *49*, 102086. [CrossRef]
14. García, L.; José, M. Recent warming in the Balearic Sea and Spanish Mediterranean coast. Towards an earlier and longer summer. *Atmósfera* **2015**, *28*, 149–160. [CrossRef]
15. Hadjinicolaou, P.; Tzyrkalli, A.; Zittis, G.; Lelieveld, J. Urbanisation and Geographical Signatures in Observed Air Temperature Station Trends Over the Mediterranean and the Middle East–North Africa. *Earth Syst. Environ.* **2023**, *7*, 649–659. [CrossRef]
16. Pastor, F.; Valiente, J.A.; Khodayar, S. A Warming Mediterranean: 38 Years of Increasing Sea Surface Temperature. *Remote Sens.* **2020**, *12*, 2687. [CrossRef]

17. Traboulsi, M.; Tolika, K.; Ch, A.; Maheras, P. Les changements des températures à Beyrouth et leurs relations avec les types de circulation atmosphérique. In *Changement Climatique, Pénurie des Ressources en Eau, Nexus Eau/Énergie et Formes d'Adaptation*; Université Hassan II: Mohammedia, Morocco, 2021. Available online: https://hal.science/hal-04878121 (accessed on 20 March 2025).
18. Oke, T.R. The energetic basis of the urban heat island. *Q. J. R. Meteorol. Soc.* **1982**, *108*, 1–24. [CrossRef]
19. Dahech, S. Le Vent à Sfax (Tunisie): Impact Sur le Climat et la Pollution Atmosphérique. Ph.D. Thesis, Paris 7 University, Paris, France, 2007. Available online: https://theses.fr/2007PA070002 (accessed on 1 January 2025).
20. Lemonsu, A.; Viguié, V.; Daniel, M.; Masson, V. Vulnerability to heat waves: Impact of urban expansion scenarios on urban heat island and heat stress in Paris (France). *Urban Clim.* **2015**, *14*, 586–605. [CrossRef]
21. EPA (U.S. Environmental Protection Agency). The Urban Heat Island Effect. 2020. Available online: https://www.epa.gov/heatislands/heat-island-trends (accessed on 20 April 2025).
22. Akbari, H.; Cartalis, C.; Kolokotsa, D.; Muscio, A.; Pisello, A.L.; Rossi, F.; Santamouris, M.; Synnefa, A.; Wong, N.H.; Zinzi, M. Local climate change and urban heat island mitigation techniques—The state of the art. *J. Civ. Eng. Manag.* **2016**, *22*, 1111934. [CrossRef]
23. Carrega, P. Topoclimatologie et Habitat. Ph.D. Thesis, Nice university, Nice, France, 1992. Available online: https://theses.fr/1992NICE2021 (accessed on 15 April 2025).
24. Sakr, S. Brises thermiques et Risque de Pollution Dans la Région de Beyrouth. Ph.D. Thesis, Aix-Marseille University, Marseille, France, 2012. Available online: https://theses.fr/2012AIXM3137 (accessed on 15 April 2025).
25. Zeinaldine, R. Aspects du Topoclimat et Pollution Atmosphérique à Zahlé (Liban Oriental). Ph.D. Thesis, Paris Cité University, Paris, France, 2024.
26. Oke, T.R.; Mills, G.; Christen, A.; Voogt, J.A. *Urban Climates*; Cambridge University Press: Cambridge, UK, 2017.
27. Cordeiro, A.; Ornelas, A.; Lameiras, J.M. The Thermal Regulator Role of Urban Green Spaces: The Case of Coimbra (Portugal). *Forests* **2023**, *14*, 2351. [CrossRef]
28. Pettitt, A.N. A Non-Parametric Approach to the Change-Point Problem. *J. R. Stat. Soc. Ser. C (Appl. Stat.)* **1979**, *28*, 126–135. [CrossRef]
29. Alexandersson, H. A homogeneity test applied to precipitation data. *J. Climatol.* **1986**, *6*, 661–675. [CrossRef]
30. Buishand, T.A. Some methods for testing the homogeneity of rainfall records. *J. Hydrol.* **1982**, *58*, 11–27. [CrossRef]
31. von Neumann, J. Distribution of the Ratio of the Mean Square Successive Difference to the Variance. *Ann. Math. Stat.* **1941**, *12*, 367–395. [CrossRef]
32. Wijngaard, J.B.; Tank, A.M.G.K.; Können, G.P. Homogeneity of 20th century European daily temperature and precipitation series. *Int. J. Climatol.* **2003**, *23*, 679–692. [CrossRef]
33. Draper, N.R.; Smith, H. *Applied Regression Analysis*; John Wiley & Sons: Hoboken, NJ, USA, 1998.
34. Feidas, H.; Makrogiannis, T.; Bora-Senta, E. Trend analysis of air temperature time series in Greece and their relationship with circulation using surface and satellite data: 1955–2001. *Theor. Appl. Climatol.* **2004**, *79*, 185–208. [CrossRef]
35. Gavrilov, M.B.; Tošić, I.; Marković, S.B.; Unkašević, M.; Petrović, P. Analysis of annual and seasonal temperature trends using the Mann-Kendall test in Vojvodina, Serbia. *Időjárás* **2016**, *120*, 183–198. Available online: https://physrep.ff.bg.ac.rs/handle/123456789/1126 (accessed on 2 April 2025).
36. Bosneagu, R.; Lupu, C.E.; Torica, E.; Lupu, S.; Vatu, N.; Tanase, V.M.; Vasilache, C.; Daneci-Patrau, D.; Scurtu, I.C. Long-term analysis of air temperatures variability and trends on the Romanian Black Sea Coast. *Acta Geophys.* **2022**, *70*, 2179–2197. [CrossRef]
37. Gadedjisso-Tossou, A.; Adjegan, K.I.; Kablan, A.K.M. Rainfall and Temperature Trend Analysis by Mann–Kendall Test and Significance for Rainfed Cereal Yields in Northern Togo. *Science* **2021**, *3*, 17. [CrossRef]
38. Liyew, C.M.; Meo, R.; Ferraris, S.; Di Nardo, E. Analysis of Diurnal Air Temperature Trends and Pattern Similarities in Highland and Lowland Stations of Italy and UK. *Int. J. Climatol.* **2024**, *44*, 5398–5417. [CrossRef]
39. Salameh, A.A.M.; Gámiz-Fortis, S.R.; Castro-Díez, Y.; Hammad, A.A.; Esteban-Parra, M.J. Spatio-temporal analysis for extreme temperature indices over the Levant region. *arXiv* **2024**. [CrossRef]
40. Onoz, B.; Bayazit, M. The power of statistical tests for trend detection. *Turk. J. Eng. Environ. Sci.* **2003**, *27*, 247.
41. Barnston, A.G.; Livezey, R.E. Classification, Seasonality and Persistence of Low-Frequency Atmospheric Circulation Patterns. *Mon. Weather. Rev.* **1987**, *115*, 1083–1126. [CrossRef]
42. Hurrell, J.W. Decadal Trends in the North Atlantic Oscillation: Regional Temperatures and Precipitation. *Science* **1995**, *269*, 676–679. [CrossRef] [PubMed]
43. Chen, W.Y.; den Dool, H.V. Sensitivity of Teleconnection Patterns to the Sign of Their Primary Action Center. *Mon. Weather. Rev.* **2003**, *131*, 2885–2899. [CrossRef]
44. Conte, M.; Giuffrida, A.; Tedesco, S. The mediterranean oscillation: Impact on precipitation and hydrology in Italy. *Suom. Akat. Julk.* **1989**, *9*, 121–137.
45. Mariotti, A.; Zeng, N.; Lau, K.-M. Euro-Mediterranean rainfall and ENSO—A seasonally varying relationship. *Geophys. Res. Lett.* **2002**, *29*, 59-1–59-4. [CrossRef]

46. Geeson, N.A.; Brandt, C.J.; Thornes, J.B. *Mediterranean Desertification: A Mosaic of Processes and Responses*; John Wiley & Sons: Hoboken, NJ, USA, 2003.
47. Palutikof, J. Analysis of Mediterranean Climate Data: Measured and Modelled. In *Mediterranean Climate. Regional Climate Studies*; Bolle, H.J., Ed.; Springer: Berlin/Heidelberg, Germany, 2003.
48. Oke, T.R. *Boundary Layer Climates*; Routledge: London, UK, 2002.
49. Faour, G.; Hanna, J.; Hammoud, B. Investigation of Thermal Heat Mapping and Vegetation Cooling Impact Using Landsat-5, -7, and -8 Imagery: A Case Study of Greater Beirut Area in Lebanon. *Environ. Sci. Proc.* **2023**, *29*, 18. [CrossRef]
50. Kaloustian, N.; Diab, Y. Effects of urbanization on the urban heat island in Beirut. *Urban Clim.* **2015**, *14*, 154–165. [CrossRef]
51. Zeinaldine, R.; Dahech, S. Topoclimatic characteristics of Zahlé (Eastern Lebanon): Thermal breezes and urban heat island phenomenon—Preliminary results. *Theor. Appl. Climatol.* **2023**, *154*, 1075–1098. [CrossRef]
52. Whiteman, C.D. Breakup of Temperature Inversions in Colorado Mountain Valleys. Ph.D. Thesis, Colorado State University, Fort Collins, CO, USA, 1980. Available online: https://ui.adsabs.harvard.edu/abs/1980PhDT.....96W (accessed on 15 April 2025).
53. Anquetin, S.; Guilbaud, C.; Chollet, J.-P. The Formation and Destruction of Inversion Layers within a Deep Valley. *J. Appl. Meteorol. Climatol.* **1998**, *37*, 1547–1560. [CrossRef]
54. Michelot, N.; Carrega, P. Topoclimatogie et pollution de l'air dans les Alpes-Maritimes: Mécanismes et conséquences en images. *EchoGéo* **2014**, *29*. [CrossRef]
55. Bokwa, A.; Hajto, M.J.; Walawender, J.P.; Szymanowski, M. Influence of diversified relief on the urban heat island in the city of Kraków, Poland. *Theor. Appl. Climatol.* **2015**, *122*, 365–382. [CrossRef]
56. Faour, G.; Mhawej, M. Mapping Urban Transitions in the Greater Beirut Area Using Different Space Platforms. *Land* **2014**, *3*, 941–956. [CrossRef]
57. Costanzini, S.; Boccolari, M.; Vega Parra, S.; Despini, F.; Lombroso, L.; Teggi, S. A comparative analysis of temperature trends at Modena Geophysical Observatory and Mount Cimone Observatory, Italy. *Int. J. Climatol.* **2024**, *44*, 4741–4766. [CrossRef]
58. Boras, M.; Herceg-Bulić, I.; Žgela, M. Urban Heat Load in a Small Mediterranean City in Recent, Extreme and Future Climate Conditions—A Case Study for the City of Dubrovnik. *Int. J. Climatol.* **2025**, *45*, e8728. [CrossRef]
59. Kalogeropoulos, G.; Dimoudi, A.; Toumboulidis, P.; Zoras, S. Urban Heat Island and Thermal Comfort Assessment in a Medium-Sized Mediterranean City. *Atmosphere* **2022**, *13*, 1102. [CrossRef]
60. Sangiorgio, V.; Bruno, S.; Fiorito, F. Comparative Analysis and Mitigation Strategy for the Urban Heat Island Intensity in Bari (Italy) and in Other Six European Cities. *Climate* **2022**, *10*, 177. [CrossRef]
61. Matthaios, V.N.; Garas, S.K.; Triantafyllou, A.G. Urban Heat Island in a Small Size Town in Northwestern Greece—A Comparison to Other Greek Areas. In *Perspectives on Atmospheric Sciences*; Karacostas, T., Bais, A., Nastos, P.T., Eds.; Springer International Publishing: Cham, Switzerland, 2017; pp. 759–765. [CrossRef]
62. Dahech, S.; Berriche, M.; Charfi, S. L'îlot de chaleur urbain à Gabès dans le contexte du changement climatique (Tunisie méridionale). Méditerranée. *Rev. Géographique Pays Méditerranéens/J. Mediterr. Geogr.* **2025**, 5627. [CrossRef]
63. Keppas, S.C.; Papadogiannaki, S.; Parliari, D.; Kontos, S.; Poupkou, A.; Tzoumaka, P.; Kelessis, A.; Zanis, P.; Casasanta, G.; de'Donato, F.; et al. Future Climate Change Impact on Urban Heat Island in Two Mediterranean Cities Based on High-Resolution Regional Climate Simulations. *Atmosphere* **2021**, *12*, 884. [CrossRef]

Disclaimer/Publisher's Note: The statements, opinions and data contained in all publications are solely those of the individual author(s) and contributor(s) and not of MDPI and/or the editor(s). MDPI and/or the editor(s) disclaim responsibility for any injury to people or property resulting from any ideas, methods, instructions or products referred to in the content.